Supplementary Information for

Last deglacial abrupt climate changes caused by meltwater pulses in the Labrador Sea

Defang You, Ruediger Stein, Kirsten Fahl, Maricel C. Williams, Daniela N. Schmidt,
Ian Nicholas McCave, Stephen Barker, Enno Schefuß, Lu Niu, Gerhard Kuhn, Frank Niessen

This document includes:

Supplementary Table 1: AMS ^{14}C dates of Core MSM12/2-5-1.
Supplementary Fig. 1: Modern hydrography of study area.
Supplementary Fig. 2: Records of lithology and bulk parameters (Core MSM12/2-5-1).
Supplementary Fig. 3: X-ray photographs of Core MSM12/2-5-1 (depth extent 500-1200 cm) showing internal structure of sediments.
Supplementary Fig. 4: P_DIP_{25} plot and scatter plot of concentrations of sea ice proxy IP_{25} versus open-water phytoplankton proxy dinosterol (Core MSM12/2-5-1).
Supplementary Fig. 5: Proxy records for sediment provenance and bottom current intensity (Core MSM12/2-5-1 and other cores referred to).
Supplementary Fig. 6: Spectral analysis record of meltwater proxy $\%C_{37:4}$ (Core MSM12/2-5-1).
Supplementary Fig. 7: Comparation between different proxy records from the North Atlantic during the last deglaciation.
Supplementary Fig. 8: Proxy records of MW4 (Core MSM12/2-5-1) versus the 8.2 ka BP cold event based on Marine 20 calibration curve.

Data availability:

All relevant data in this supplementary information is available at PANGAEA Data Publisher (https://doi.org/10.1594/PANGAEA.952329)[1]

Supplementary Table 1 AMS ^{14}C dates of Core MSM12/2-5-1.

Lab ID	Depth/cm	Species	AMS ^{14}C age (yr.)	△R	Calib. age median (yr. BP)	Model age median (yr. BP)
SUERC-45889*	4.75	*N. pachyderma*	2082±35	0±200	1669	1899
SUERC-47577	108.5	*N. pachyderma*	3450±38	0±200	3314	3281
SUERC-45890	200.5	*N. pachyderma*	4227±37	0±200	4319	4420
SUERC-47579	300.5	*N. pachyderma*	5473±39	0±200	5857	5875
SUERC-47579	390.5	*N. pachyderma*	6737±37	0±200	7236	7208
AWI-6946.1.1**	440.5	*N. pachyderma*	7520±85	0±200	7986	7860
AWI-6947.1.1	470.5	*N. pachyderma*	7933±86	0±200	8420	8123
AWI-6948.1.1	500.5	*N. pachyderma*	8115±84	0±200	8641	8334
AWI-6949.1.1	600.5	*N. pachyderma*	8134±84	0±200	8664	8852
AWI-6950.1.1	620.5	*N. pachyderma*	8298±83	0±200	8849	8962
SUERC-45891	650.5	*N. pachyderma*	8449±38	0±200	9038	9154
SUERC-47582	720.5	*N. pachyderma*	9049±40	0±200	9793	9625
AWI-5788.1.1	749.5	*N. pachyderma*	9096±122	0±200	9847	9802
AWI-5789.1.1	799.5	*N. pachyderma*	9585±117	0±200	10464	10099
AWI-5793.1.1	919.5	*N. pachyderma*	9831±127	0±200	10767	10680
AWI-5794.1.1	929.5	*N. pachyderma*	9606±120	0±200	10490	10729
AWI-5795.1.1	952.5	*N. pachyderma*	9641±119	0±200	10534	10855
AWI-5798.1.1	999.5	*N. pachyderma*	9860±119	0±200	10802	11131
AWI-5799.1.1	1029.5	*N. pachyderma*	10029±125	0±200	11008	11409
AWI-5800.1.1	1059.5	*N. pachyderma*	10428±128	0±200	11627	11744
AWI-5803.1.1	1108.5	*N. pachyderma*	10543±129	0±200	11788	12275
AWI-6484.1.1	1114.5	*N. pachyderma*	10621±100	0±200	11908	12308
AWI-6485.1.1	1118.5	*N. pachyderma*	11130±101	0±200	12611	12332
AWI-6486.1.1	1123.5	*N. pachyderma*	11141±94	0±200	12626	12635
AWI-6487.1.1	1127.5	*N. pachyderma*	11752±95	0±200	13213	12969
AWI-5952.1.1	1130.5	*N. pachyderma*	11854±131	0±200	13320	13217
SUERC-47583	1140.5	*N. pachyderma*	12379±43	0±200	13869	14027
SUERC-51888	1150.5	*N. pachyderma*	12975±44	0±200	14794	14374
AWI-6488.1.1	1153.5	*N. pachyderma*	12942±102	0±200	14742	14483
AWI-6489.1.1	1155.5	*N. pachyderma*	12671±102	0±200	14356	14555
AWI-6490.1.1	1157.5	*N. pachyderma*	12518±106	0±200	14086	14629
AWI-6491.1.1	1159.5	*N. pachyderma*	12721±106	0±200	14434	14699
AWI-5954.1.1	1160.5	*N. pachyderma*	12544±120	0±200	14135	14851
AWI-6492.1.1	1162.5	*N. pachyderma*	12972±105	0±200	14789	15387
AWI-5955.1.1	1165.5	*N. pachyderma*	13965±135	0±200	16361	16192
AWI-5956.1.1	1167.5	*N. pachyderma*	14937±147	0±200	17683	16731
SUERC-47584	1170.5	*N. pachyderma*	15386±51	0±200	18212	17542
SUERC-51887	1190.5	*N. pachyderma*	17007±57	0±200	20031	20358

* AMS ^{14}C dates have been carried out at the NERC Radiocarbon Laboratory at SUERC (Scottish Universities Environment Research Centre, the University of Glasgow). They were recalculated from the unpublished data of the PhD dissertation of Williams[2].

** AMS ^{14}C dates were measured at the Alfred Wegener Institute, Bremerhaven.

A global mean reservoir age (R=405 years) was used for calibration to keep consistency with most of studies in the open North Atlantic regions (e.g., Refs.[3,4]), and a △R of 0 ± 200 years was applied to account for the reservoir age variations, which is in line with other studies in the North Atlantic (cf., Refs.[5–7]).

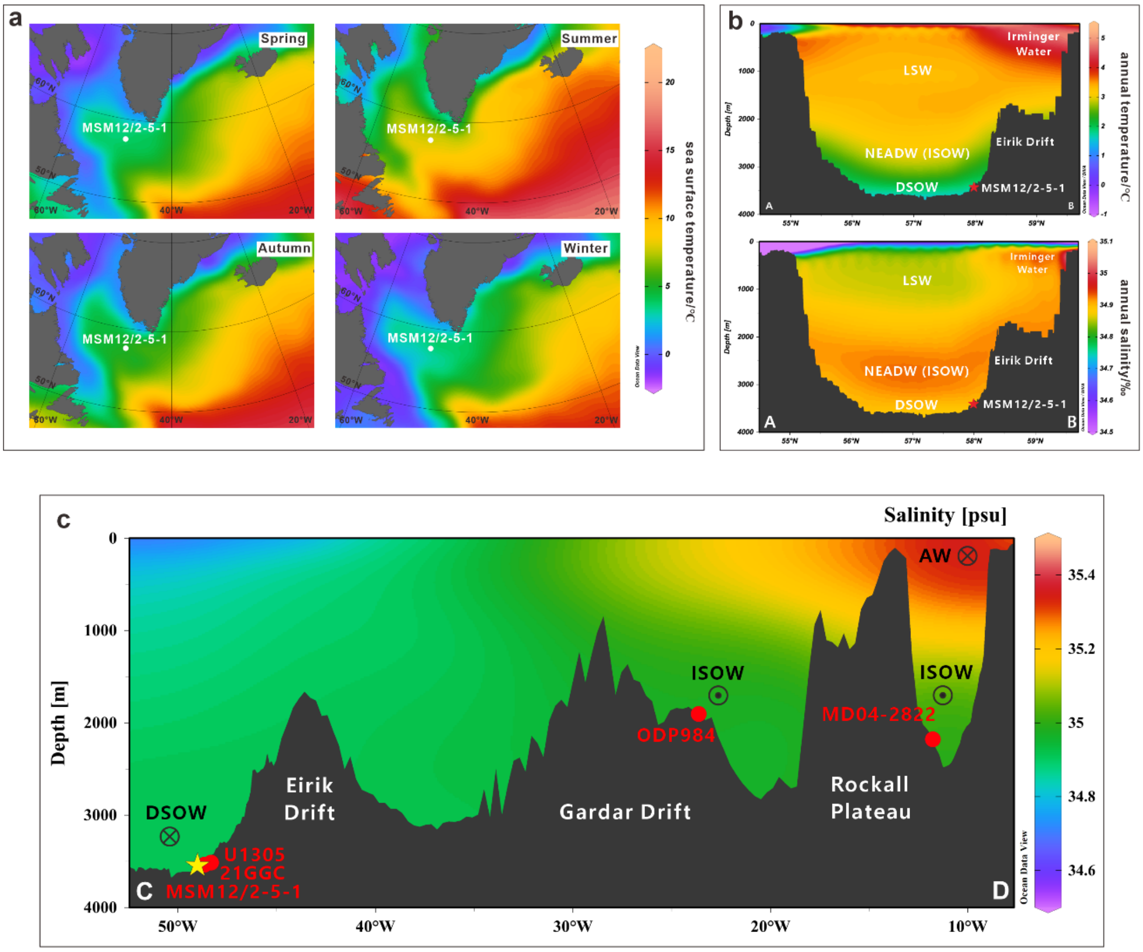

Supplementary Fig. 1 Modern hydrography of study area.

(**a**) Modern seasonal variability of SST in the subpolar western North Atlantic regions; (**b**) Vertical distribution of water masses in terms of temperature and salinity at profile A to B. northeastern Atlantic Deep Water (NEADW) in the Labrador Sea is derived from ISOW; (**c**) salinity profile in the North Atlantic from C to D. For location of profiles A to B and C to D see map of Figure 1. Data is from World Ocean Atlas 2018 (https://odv.awi.de/data/ocean/). Profiles were produced with Ocean Data View software (https://odv.awi.de).

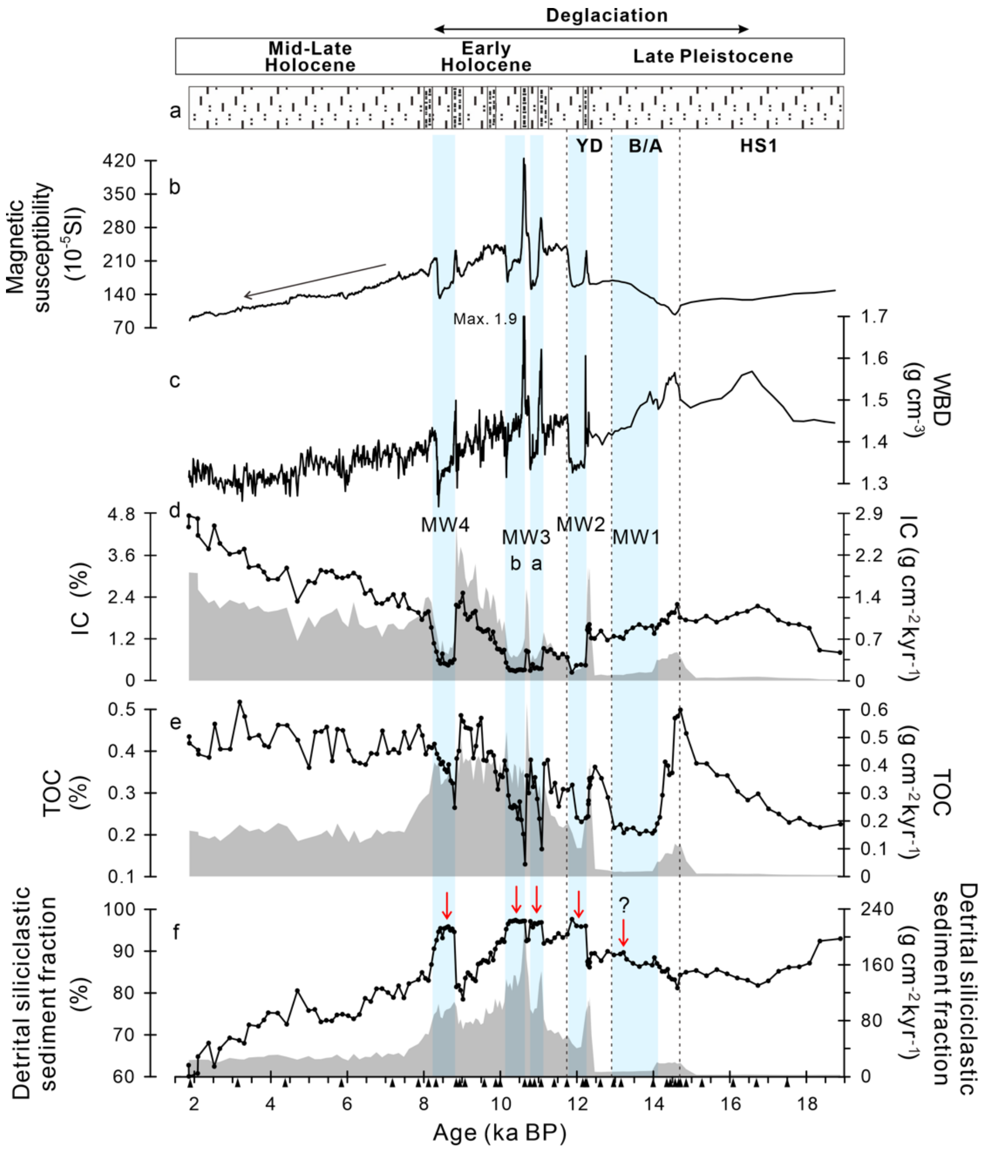

Supplementary Fig. 2 Records of lithology and bulk parameters (Core MSM12/2-5-1).

(**a**) Illustration of core lithology[8]; (**b**) Magnetic susceptibility (MS); the decreasing trend of MS values since the middle to late Holocene are explained by increased input of carbonate and decreased input of siliciclastic material; (**c**) Wet bulk density (WBD); (**d**) Content (line) and accumulation rate (shading) of inorganic carbon (IC); (**e**) Content and accumulation rate of TOC; (**f**) Content and accumulation rate of detrital siliciclastic sediment fraction (bulk sediment without TOC and carbonate). Concentration and accumulation rate of carbonate were calculated assuming that calcite is the predominant carbonate phase ($CaCO_3$=(TC-TOC) × 8.333). As biogenic opal is insignificant in study area[9], this predominantly represent the terrigenous/detrital siliciclastic sediment fraction. Red arrows indicate higher non-biogenic fraction input corresponding to peaks of sedimentation rate (Fig. 2). Black triangles mark available AMS^{14}C dates.

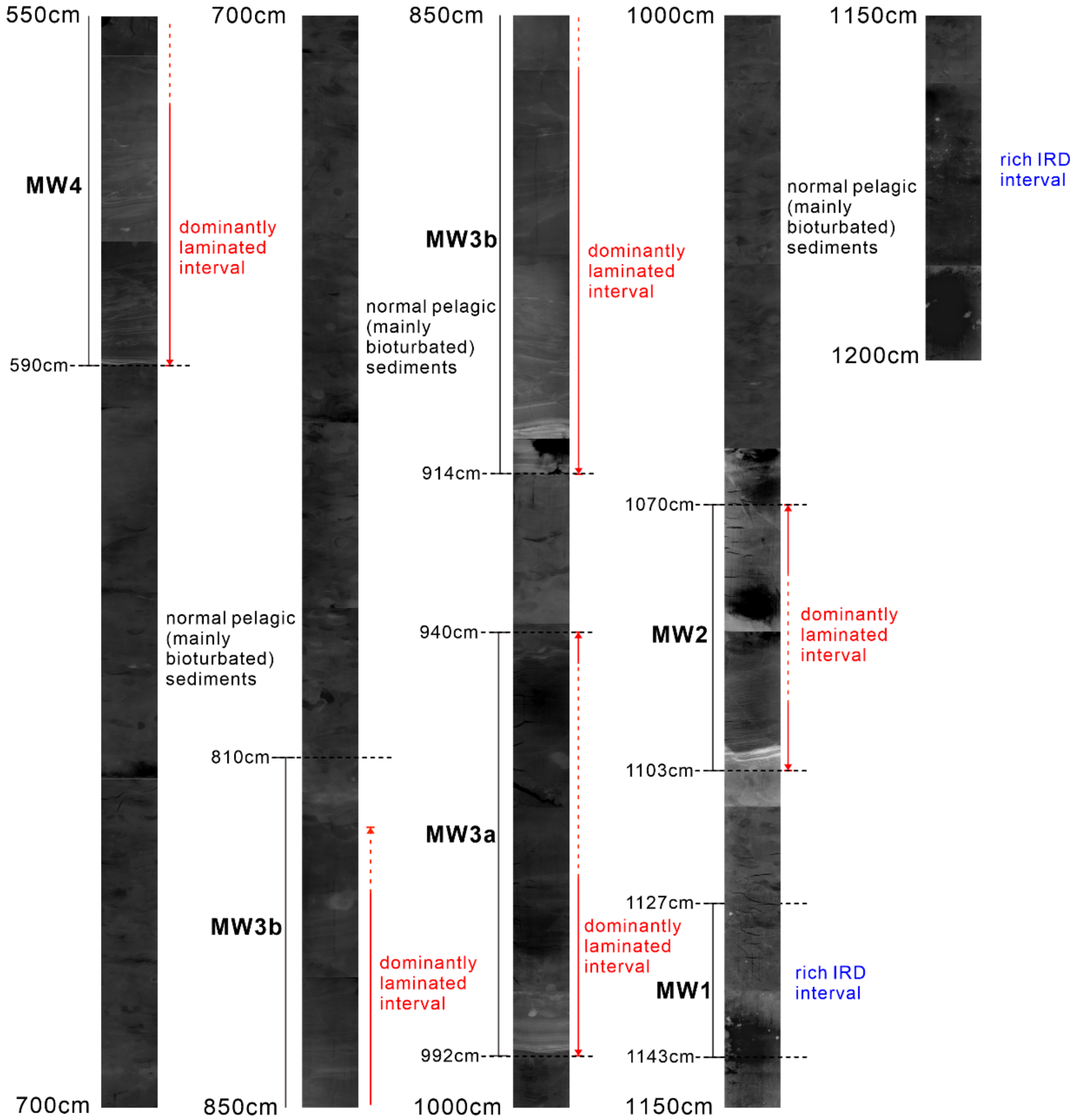

Supplementary Fig. 3 X-ray photographs of Core MSM12/2-5-1 (depth extent 500-1200 cm) showing internal structure of sediments.

MW1 to MW4 are characterised by silty clay/clayey silt laminations (interpreted as plumites) related to meltwater plumes as shown in the X-ray photographs. The dominant laminated intervals and IRD-rich intervals are highlighted. The bioturbated sediments are intercalated by dominant laminated intervals. For source of X-ray photographs of core MSM12/2-5-1 we refer to Ref.[10].

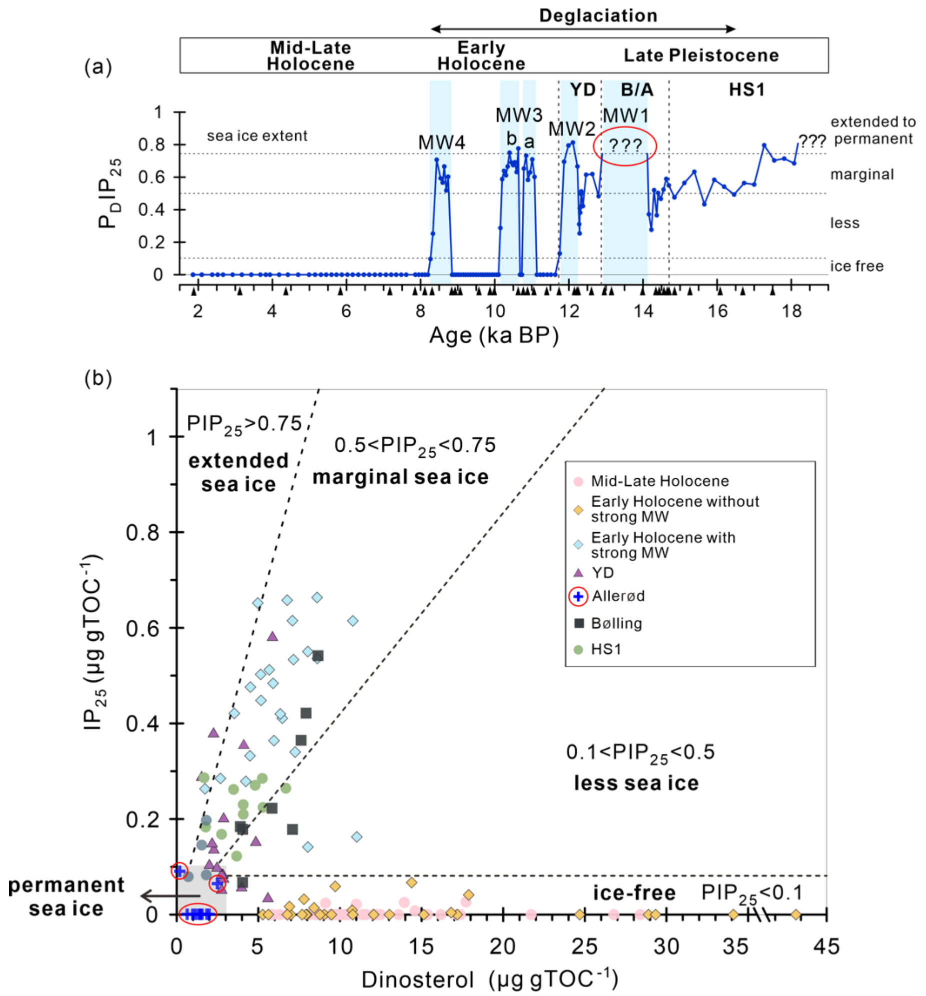

Supplementary Fig. 4 (a) P_DIP_{25} plot and (b) Scatter plot of concentrations of sea ice proxy IP_{25} versus open-water phytoplankton proxy dinosterol (Core MSM12/2-5-1).

Classification of sea ice cover according to Müller et al.[11]. For zero or minimum concentrations of IP_{25} and phytoplankton biomarkers, i.e., for the data points in the light grey background square close to the origin of the plot (**b**), reliable P_DIP_{25} cannot be calculated (highlighted by question marks in (**a**)) and set to "1" in the original work by Müller et al.[11], assuming a permanent sea ice cover. Such interpretation is unrealistic in our case as SST values are well above 0 °C during these time intervals (for details see the text). Black triangles mark available AMS^{14}C dates.

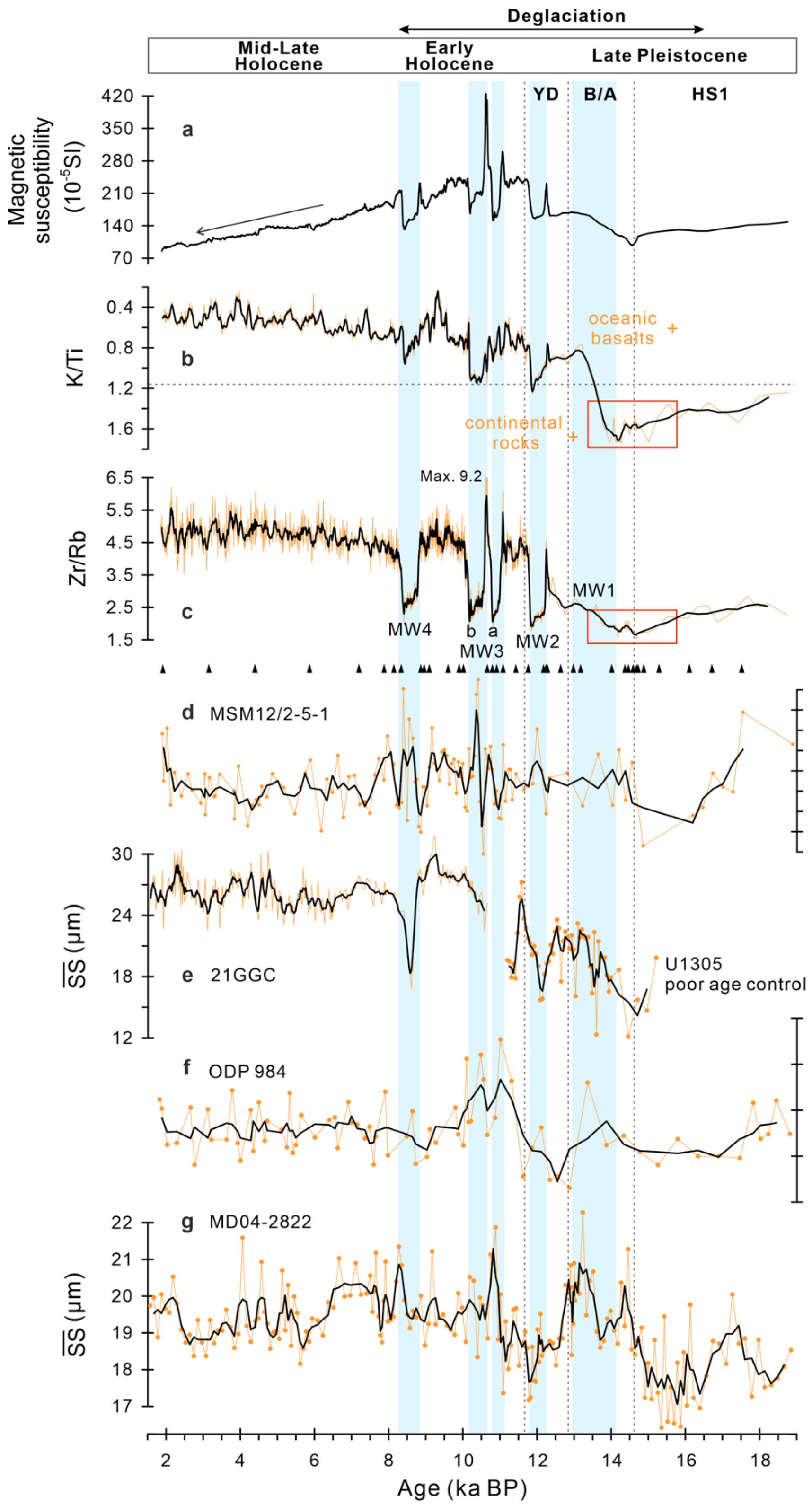

Supplementary Fig. 5 Proxy records for sediment provenance and bottom current intensity.
Records from Core MSM12/2-5-1 (**a-d**) and reference cores (**e-g**). (**a**) Magnetic susceptibility; the decreasing trend of MS values since the middle to late Holocene are explained by increased input of carbonate and decreased input of siliciclastic material (cf., Supplementary Fig. 2); (**b**) XRF-K/Ti ratios as proxy for sediment provenance. K might be indicative for input of weathering products of continental rocks[12], whereas Ti is more related to weathering products of basalts, e.g., from Iceland/eastern Greenland[13]. Red box shows high input of continental rocks; (**c**) XRF-Zr/Rb ratios as proxy for coarse- versus fine-grained matter. The ratios during the late HS1 to Bølling periods could be highly influenced by increased input of continental sediments, causing high K but also high Rb values[12,14] and resulting in higher K/Ti and lower Zr/Rb ratios as shown in our records; (**d**) Sortable silt mean size ($\overline{SS}$) record of Core MSM12/2-5-1; black line shows 3 points running average of $\overline{SS}$ values; (**e**) $\overline{SS}$ record of Core 21GGC and IODP Site 1305 from Eirik Drift[15]; (**f**) $\overline{SS}$ record of ODP Site 984 from Gardar Drift[16]; (**g**) $\overline{SS}$ record of Core MD04-2822 from Rockall Plateau[17]. Black triangles mark available AMS^{14}C dates.

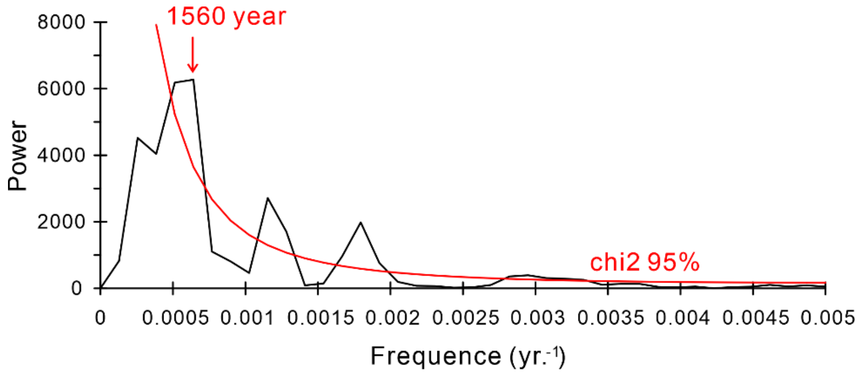

Supplementary Fig. 6 Spectral analysis record of meltwater proxy %$C_{37:4}$ (Core MSM12/2-5-1).
%$C_{37:4}$ data during 14-8.2 ka BP was used for spectral analysis. The red line indicates 95% confidence level. The 1560-year cycle shows the highest power.

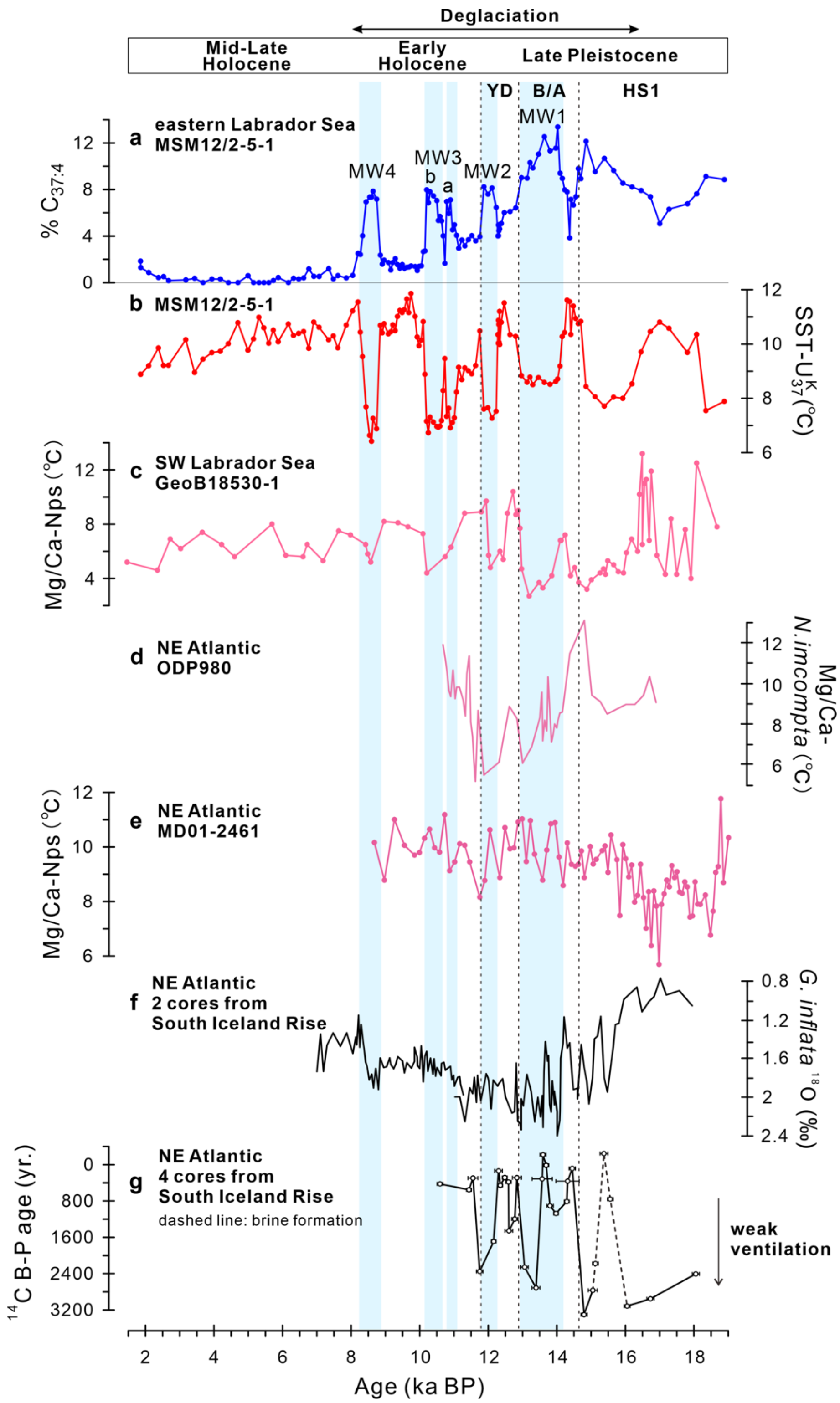

Supplementary Fig. 7 Comparation between different proxy records from the North Atlantic during the last deglaciation.

(**a**) Percentage of $C_{37:4}$ as proxy for meltwater discharge from Core MSM12/2-5-1; (**b**) SST reconstruction based on U^K_{37} from Core MSM12/2-5-1; (**c**) Subsurface temperature record based on Nps-Mg/Ca ratios from Core GeoB18530-1[18]; (**d**) Subsurface temperature estimates based on Ma/Ca ratios of *N. incompta* from ODP Site 980[19]; (**e**) Subsurface temperature record based on Nps-Mg/Ca ratios from Core MD01-2461[20]; (**f**) δ^{18}O record of *G. inflata* from South Iceland Rise[21]; (**g**) Difference in ^{14}C between benthic and planktic foraminifera from South Iceland Rise, indicating the ventilation in the North Atlantic[22]. The horizontal error bars represent the propagated uncertainties of ^{14}C measurement.

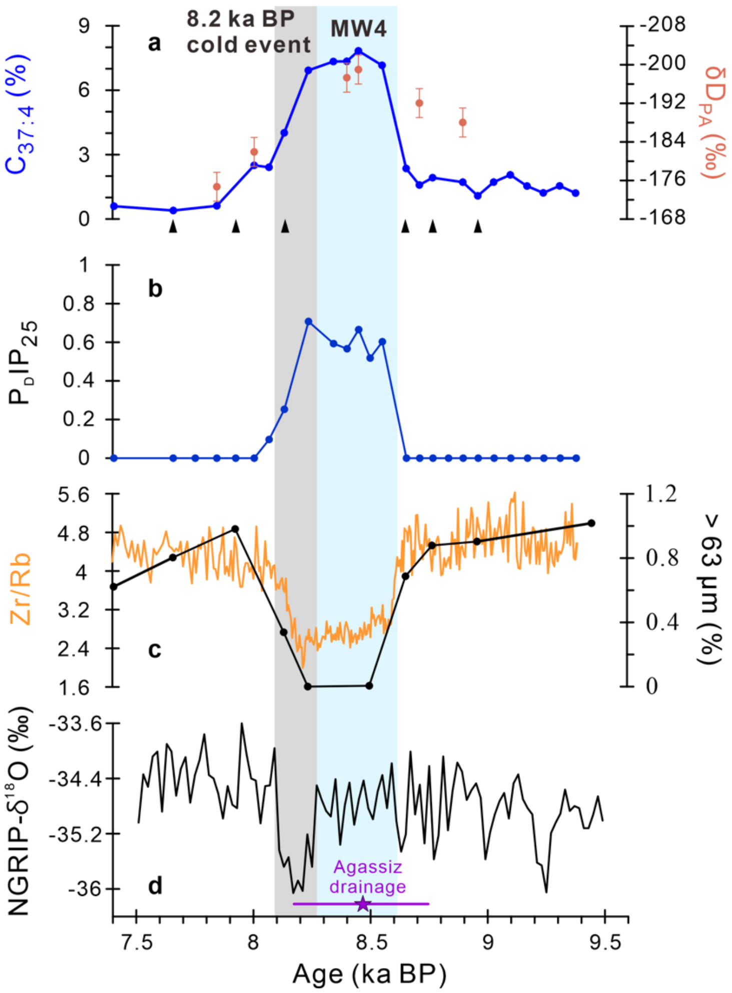

Supplementary Fig. 8 Proxy records of MW4 (Core MSM12/2-5-1) versus the 8.2 ka BP cold event based on Marine 20 calibration curve[23].

(**a-c**) Proxy records for abrupt change in MW4 from Core MSM12/2-5-1. (**a**) %$C_{37:4}$ and stable hydrogen isotope composition of palmitic acid (δD_{PA}) as proxies for meltwater discharge (with higher %$C_{37:4}$ and lower δD_{PA} representing lower salinity). Vertical error bars represent the standard deviation of the δD_{PA} measurements (3 ‰); (**b**) P_DIP_{25} as proxy for sea ice extent; (**c**) XRF-Zr/Rb ratios indicating coarse versus fine-grained matter; percentage of coarse fraction (>63 µm); (**d**) Greenland Ice Core record[24]. The age of ice core was calculated to cal. ka BP from GICC05 age. The purple star indicates the age for Lake Agassiz drainage event: 8.47 ka BP with 1σ uncertainties (purple line, 8.16-8.74 ka BP)[25]. Light blue shading shows the meltwater event 4 (MW4), whereas grey shading indicates the 8.2 ka BP cold event shown in the Greenland Ice Core. Based on the Marine 20 calibration, the 8.2 ka BP cold event probably occurred at the end of MW4. That means, in comparison to the Marine 13 calibration, all three proxy records become around 200 years younger (see Fig. 5 in the main text). Black triangles mark available AMS^{14}C dates.

Supplementary references

1. You, D. *et al.* Biomarker, bulk parameter, XRF data of sediment core MSM12/2-5-1 from the Labrador Sea. *PANGAEA* https://doi.org/10.1594/PANGAEA.952329 (2022).
2. Williams, M. C. The Pelagic Record of Ocean Acidification. (Doctoral dissertation, University of Bristol, 2015).
3. Ng, H. C. *et al.* Coherent deglacial changes in western Atlantic Ocean circulation. *Nat. Commun.* **9**, 1–10 (2018).
4. Zhao, N. *et al.* Glacial–interglacial Nd isotope variability of North Atlantic Deep Water modulated by North American ice sheet. *Nat. Commun.* **10**, 1–10 (2019).
5. Toucanne, S. *et al.* Millennial-scale fluctuations of the European Ice Sheet at the end of the last glacial, and their potential impact on global climate. *Quat. Sci. Rev.* **123**, 113–133 (2015).
6. Oppo, D. W., Curry, W. B. & McManus, J. F. What do benthic $\delta^{13}C$ and $\delta^{18}O$ data tell us about Atlantic circulation during Heinrich Stadial 1? *Paleoceanography* **30**, 353–368 (2015).
7. Andrews, J. T. *et al.* Sea ice, ice-rafting, and ocean climate across Denmark Strait during rapid deglaciation (~16–12 cal ka BP) of the Iceland and East Greenland shelves. *J. Quat. Sci.* **33**, 112–130 (2018).
8. Uenzelmann-Neben, G. The expedition of the research vessel" Maria S. Merian" to the Labrador Sea in 2009 (MSM 12/2) Reykjavik-Reykjavik 17. June-13. July 2009. *Reports Polar Mar. Res.* **599**, (2009).
9. Bohrmann, G. & Stein, R. Biogenic silica at ODP Site 647 in the southern Labrador Sea: occurrence, diagenesis, and paleoceanographic implications. *Proc. Ocean Drill. Progr. Sci. Results* **105**, 155–170 (1989).
10. Stein, R. Documentation of sediment core MSM12:647-1 (MSM12/2-5-1). Alfred Wegener Institute, Helmholtz Centre for Polar and Marine Research, Bremerhaven. *PANGAEA* (2010) doi:https://doi.org/10.1594/PANGAEA.733357.
11. Müller, J. *et al.* Towards quantitative sea ice reconstructions in the northern North Atlantic: A combined biomarker and numerical modelling approach. *Earth Planet. Sci. Lett.* **306**, 137–148 (2011).
12. Grützner, J. & Higgins, S. M. Threshold behavior of millennial scale variability in deep water hydrography inferred from a 1.1 Ma long record of sediment provenance at the southern Gardar Drift. *Paleoceanography* **25**, PA4204 (2010).
13. Ballini, M., Kissel, C., Colin, C. & Richter, T. Deep-water mass source and dynamic associated with rapid climatic variations during the last glacial stage in the North Atlantic: A multiproxy investigation of the detrital fraction of deep-sea sediments. *Geochemistry, Geophys. Geosystems* **7**, Q02N01 (2006).
14. Dypvik, H. & Harris, N. B. Geochemical facies analysis of fine-grained siliciclastics using Th/U, Zr/Rb and (Zr + Rb)/Sr ratios. *Chem. Geol.* **181**, 131–146 (2001).
15. Henderson, S. S. Tracking Deep-Water Flow On Eirik Drift Over The Past 160 Kyr: Linking Deep-Water Changes To Freshwater Fluxes. (Doctoral dissertation, Rutgers The State University of New Jersey, 2009).
16. Praetorius, S. K., McManus, J. F., Oppo, D. W. & Curry, W. B. Episodic reductions in bottom-water currents since the last ice age. *Nat. Geosci.* **1**, 449–452 (2008).
17. Channell, J. E. T. *et al.* Magnetic record of deglaciation using FORC-PCA, sortable-silt grain size, and magnetic excursion at 26 ka, from the Rockall Trough (NE Atlantic). *Geochemistry Geophys. Geosystems* **17**, 1823–1841 (2016).
18. Max, L., Nürnberg, D., Chiessi, C. M., Lenz, M. M. & Mulitza, S. Subsurface ocean warming preceded Heinrich Events. *Nat. Commun.* **13**, 1–8 (2022).
19. Benway, H. M., McManus, J. F., Oppo, D. W. & Cullen, J. L. Hydrographic changes in the eastern subpolar North Atlantic during the last deglaciation. *Quat. Sci. Rev.* **29**, 3336–3345 (2010).
20. Peck, V. L., Hall, I. R., Zahn, R. & Elderfield, H. Millennial-scale surface and subsurface paleothermometry from the northeast Atlantic, 55-8 ka BP. *Paleoceanography* **23**, PA3221 (2008).
21. Thornalley, D. J. R., McCave, I. N. & Elderfield, H. Freshwater input and abrupt deglacial climate change in the North Atlantic. *Paleoceanography* **25**, PA1201 (2010).
22. Thornalley, D. J. R., Barker, S., Broecker, W. S., Elderfield, H. & McCave, I. N. The deglacial evolution of north atlantic deep convection. *Science.* **331**, 202–205 (2011).
23. Heaton, T. J. *et al.* Marine20 - the marine radiocarbon age calibration curve (0-55,000 cal BP). *Radiocarbon* **62**, 779–820 (2020).
24. Svensson, A. *et al.* A 60 000 year Greenland stratigraphic ice core chronology. *Clim. Past* **4**, 47–57 (2008).
25. Barber, D. C. *et al.* Forcing of the cold event of 8,200 years ago by catastrophic drainage of Laurentide lakes. *Nature* **400**, 344–348 (1999).